Materials Science Forum
ISSN: 1662-9752, Vols. 196-201, pp 1481-1490
doi:10.4028/www.scientific.net/MSF.196-201.1481

Online: 1995-11-21

POSITRON-ANNIHILATION 2D-ACAR STUDY OF DIVACANCY AND VACANCY- OXYGEN PAIRS in Si

Masayuki Hasegawa[1], Toshinobu Chiba[2], Atsuo Kawasuso[1], Takashi Akahane [2], Masashi Suezawa[1], Sadae Yamaguchi[1] and Koji Sumino[1]
[1] Institute for Materials Research, Tohoku University, Sendai 980-77, JAPAN
[2] National Institute for Research in Inorganic Materials, Namiki 1-1, Tsukuba-shi, Ibaraki 305, JAPAN

Keywords: Positron Annihilation, Angular Correlation, Silicon, Divacancy, Vacancy- Oxygen Complex

Abstracts. Two-dimensional angular correlation of positron annihilation radiation (2D-ACAR) experiments have been performed on electron-irradiated Si single crystals containing divacancies with the definite charge states, V_2^{-2}, V_2^{-1} and V_2^{0}, from 15K to 295K. The 2D-ACAR spectra of unirradiated crystals have been also obtained and show characteristic anisotropies. Using these anisotropies, the 2D-ACAR spectra associated with the divacancies are separated from the partial bulk contribution. The 2D-ACAR spectra for the various charge states are practically isotropic and are very close to each other. However, using a specimen with oriented divacancies V_2^{-1}, we have obtained a small but definite anisotropy from the divacancies V_2^{-1}. The small increase in the FWHM width of the 2D-ACAR spectra from the divacancies is observed with decreasing temperature. The trapped fractions at the divacancies increase remarkably with decreasing temperature, not only for negative but also neutral divacancies. The 2D-ACAR spectra from vacancy-oxygen complexes is also obtained. These experimental 2D-ACAR spectra are expected to provide useful and potential information on electronic and atomistic structures of the divacancies in Si and need theoretical calculations, such as first-principle ones.

Introduction

In recent years positron annihilation experiments have emerged as a powerful tool for the studies of vacancy-type defects in semiconductors [1-5]. Among them two dimensional angular correlation of positron annihilation radiation (2D-ACAR) technique has been used in the studies of vacancy-type defects in semiconductors; it provides us with detailed momentum distribution of the electron-positron pairs [6-14]. The 2D-ACAR experiments have been successfully applied to vacancies in GaAs [8-11] and their results were in good agreement with theoretical results by the first-principle calculations using the Car-Parinello method [15]. Our preliminary studies on divacancies in Si with the 2D-ACAR method also show very interesting information, such as nearly the same momentum distribution for the different charge states [12,13]. Then we expect to open up a new field, the 2D-ACAR applied to atomic and electronic structures of defects in semiconductors.

The objective of the present work is to get further information about the 2D-ACAR spectra from the divacancies with the definite charge state in the floating zone grown Si (FZ-Si): neutral (V_2^{0}), single-minus (V_2^{-1}) or double-minus (V_2^{-2}). Especially we prepared a sample with oriented V_2^{-1} and obtained the anisotropies of 2D-ACAR spectra from the trapped positrons, which should contain information about electronic states of V_2^{-1}. Furthermore we employed also Czochralski grown Si (CZ-Si) to study the 2D-ACAR momentum distribution from vacancy-oxygen complexes.

Experimental

The crystals in this study were grown by the floating zone method (FZ-Si), unless otherwise stated. The FZ-Si crystals were bombarded with 15 MeV electrons at room temperature to introduce divacancies. To obtain the different charge states for divacancies, n- and p-type crystals with appropriate content of dopants, P or B, were irradiated up to $8x10^{17}$ e/cm^2. Since the monovacancies are mobile at room temperature, they were annealed out or stabilized themselves by forming divacancies or vacancy-impurity pairs. Concentration of tri- or higher multi-vacancy clusters were negligible at the present irradiation condition [16-18]. The divacancies has three deep levels in the band gap, E(0/+) = vb +0.25eV, E(-1/0)

Table 1. Characteristics of FZ-Si specimens irradiated with 15MeV electrons at room temperature. The Fermi levels were obtained from Hall coefficient measured at room temperature.

Specimen	Charge states	Dopant conc. (cm^{-3})	Fluence (e/cm^2)	V_2 conc. (cm^{-3})	Fermi level (eV)	Remarks
A	V_2^{-2}	P:1.7×10^{16}	3.0×10^{16}	8×10^{14}	E_C-0.17	150℃ × 0.5h annealed
B	V_2^{-1}	P:1.7×10^{16}	5.0×10^{17}	7×10^{15}	E_C-0.34	250℃ × 1h annealed
C	V_2^{0}	B:4.0×10^{14}	3.0×10^{17}	3×10^{16}	E_V+0.40	As irradiated

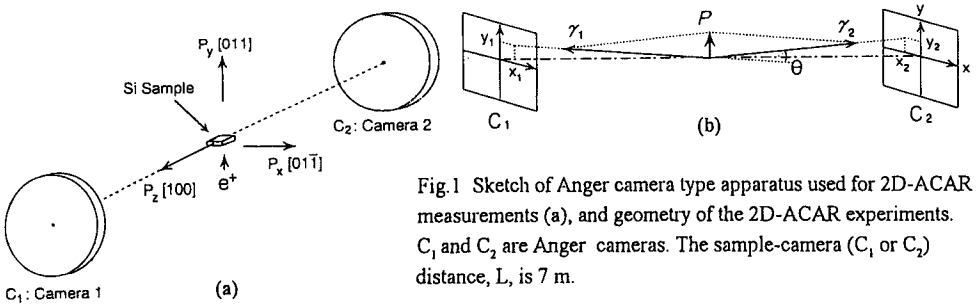

Fig.1 Sketch of Anger camera type apparatus used for 2D-ACAR measurements (a), and geometry of the 2D-ACAR experiments. C_1 and C_2 are Anger cameras. The sample-camera (C_1 or C_2) distance, L, is 7 m.

= cb -0.41eV, E(-2/-1) = cb- 0.25eV, where vb is the top of the valence band and cb is the bottom of the conduction band [19]. Depending on the relative positions of these energy levels and the Fermi levels, the divacancies can take four charge states, +1, 0, -1 or -2. After the electron irradiation, appropriate heat treatments were employed to remove vacancy-phosphor pairs in the n-type specimens. From the Hall coefficient measurements we confirmed the charge states of the divacancies [12,13]. The charge states are listed in Table 1 together with specimen characteristics. Furthermore in order to obtain the anisotropy of the 2D-ACAR spectrum of the divacancy component, the sample containing divacancies with the aligned direction in the lattice was prepared. This was achieved by stress alignment at elevated temperature; the crystals was compressed along [011] axis to 500 kg/cm^2 at 170℃ for 1h, then cooled to room temperature with stress on [20]. The degree of alignment, n_{in}/n_{out}, is estimated to be about 1.5, where n_{in} and n_{out} are population of the divacancies in (011) plane and out of the plane, respectively. In order to obtain 2D-ACAR spectra from vacancy-oxygen complex, CZ-Si samples were irradiated with 3MeV electrons to a dose of $1x10^{18}$ e/cm^2 below 50℃ and subsequently annealed at 300℃ to remove divacancies [21].

The 2D-ACAR spectra were obtained with the 2D-ACAR machine of Anger camera type, as sketched in Fig. 1(a), at the National Institute for Research in Inorganic Materials. The 2D-machine uses a pair of scintillation cameras (Hitachi RC-135DF), each of which has NaI(Tl) scintillator (40 cm diameter and 9mm thickness) coupled with 61 photomultiplier tubes. The positional resolution of 511keV annihilation photons is typically 2.1mm within the active area, 35 cm in diameter, of the camera. The two cameras are situated symmetrically on either side of a source- cryostat: the distance between the sample and each camera, L, is 7 m. A ^{22}Na positron source with an activity of 1.3 GBq, placed 5 mm below each sample, was used. The coincidence timing resolution was 26ns (FWHM) and coincidence counting rate is 100 - 200 cps. The total coincidence counts of 3 - 6 $x10^7$ were accumulated in 3 to 5 days. The angular range is 36 x 36 $mrad^2$ with the bin size of 0.2 x0.2 $mrad^2$. Positron lifetime measurements were also carried out to get positron annihilation rate at divacancies using a conventional time spectrometer [13]; the annihilation rate is given by the reciprocal of positron lifetime.

2D-ACAR Spectra for Bulk and Divacancy Components

The annihilating pair of a positron and an electron with total momentum **p** emits two photons, γ_1 and γ_2, in almost opposite direction as shown in Fig.1(b). The annihilation photons, conveying the

center-of-mass momentum of the annihilating pair (**p**), are detected in coincidence at positions (x_1 , y_1) in the Camera C_1 and (x_2 , y_2) in the Camera C_2. The angular deviation from anticollinearity , θ , is related to the x (p_x) and y (p_y) components of the annihilating pair as follows,

$$p_x = mc\,\theta_x, \quad p_y = mc\,\theta_y,$$

where

$$\theta_x = (x_1 + x_2)/L, \quad \theta_y = (y_1 + y_2)/L,$$

and m is the electron rest mass and c is the speed of light. In the units of mc, momentum is expressed in mrad. The 2D-ACAR momentum distribution spectrum $N(p_x, p_y)$, which is a frequency distribution of observing (p_x, p_y), corresponds the projection along p_z direction of the 2 γ -momentum density $\rho^{2\gamma}(\mathbf{p})$,

$$N(p_x, p_y) = \text{const.} \cdot \int \rho^{2\gamma}(\mathbf{p})dp_z$$

In Fig. 2 typical 2D-ACAR spectra at 15K are shown for [011] projection: (a) an unirradiated FZ-Si specimen, and (c) the electron-irradiated FZ-Si specimen containing neutral divacancies V_2^0 (the specimen C in Tab. 1). The 2D-ACAR spectrum of the unirradiated specimen shows large anisotropies owing to the fact that the 3p-orbitals on the neighboring sites of Si tend to have opposite phases in order to form covalent bonding [24]. However, the 2D-ACAR spectrum of the irradiated specimen C shows only a small anisotropy, which suggests very isotropic 2D-ACAR spectrum from the positrons trapped at the divacancies.

The 2D-ACAR spectra can be decomposed into a centrally symmetric isotropic part and anisotropy. Fig. 2(b) shows the anisotropic part defined as,

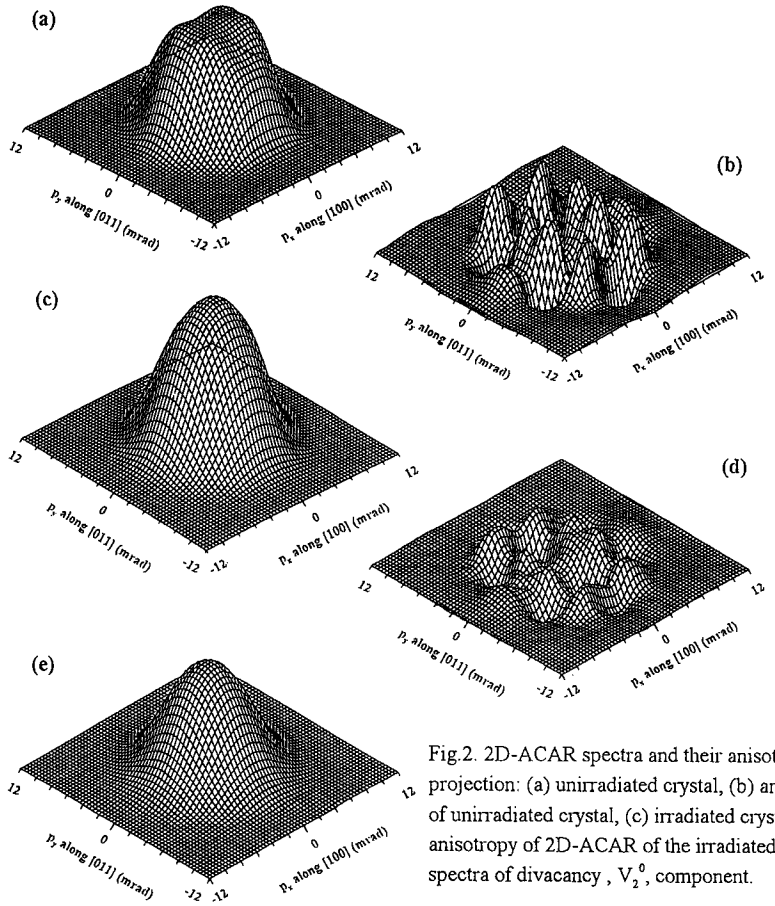

Fig.2. 2D-ACAR spectra and their anisotropies with [0$\bar{1}$1] projection: (a) unirradiated crystal, (b) anisotropy of the 2D-ACAR of unirradiated crystal, (c) irradiated crystal containing V_2^0, (d) anisotropy of 2D-ACAR of the irradiated crystal, and (e) 2D-ACAR spectra of divacancy , V_2^0, component.

$$A(p_x, p_y) = N(p_x, p_y) - C(p),$$

where C(p) is obtained by cylindrically averaging the 2D-ACAR spectrum around the center and described by a radial function in the momentum space and $p = (p_x^2 + p_y^2)^{1/2}$. The anisotropies of the 2D-ACAR spectra of Fig. 2(a) and (c) are shown in Fig.2 (b) and (d) respectively. In Fig. 2 (b) the anisotropy of the unirradiated specimen exhibits characteristic two-fold symmetry which reflects the nature of the Si-Si bonding in the crystal as stated above. We found that the anisotropies for the specimens C (V_2^0), B (V_2^{-1}) and A (V_2^{-2}) do not change their shapes beyond the uncertainty of the measurements, but only differ in their amplitudes. Furthermore the anisotropies exhibit almost the same shape, with marked reduction in their amplitudes, as that of unirradiated specimen as seen, for example, in Fig.2 (b) and (d). Therefore, we can assume almost all the anisotropies of the irradiated specimens are due to the contribution of the bulk (perfect crystal) component contained in the irradiated specimens. For example, the anisotropy of the specimen C is 40.3% of that for the unirradiated specimen in the overall amplitude. This suggests that 40.3% of the positrons in the specimen C annihilate with valence electrons in the bulk state, while the remaining 59.7% of the positrons are trapped at the divacancies and annihilate with electrons associated with the divacancies. Then we can assume that the 2D-ACAR spectrum of Fig. 2(c) consists of two contribution: the bulk component with a fraction of 40.3% and the divacancy component with the remainig fraction of 59.7%. These fractions are almost consistent with that from lifetime experiments as stated later. In Fig. 2(e), the divacancy component obtained by subtraction of the bulk component from Fig. 2(c) is shown. The resulting 2D-ACAR spectrum from the neutral divacancies shows a quite isotropic distribution. The 2D-ACAR spectra for negatively charged divacancies, V_2^{-1} and V_2^{-2}, also show very isotropic 2D-ACAR distribution [13].

The isotropic parts of the 2D-ACAR spectra of [011] projection for the divacancy components are shown in Fig.3(a) together with the bulk component. The 2D-ACAR spectra from the divacancies V_2^0, V_2^{-1} and V_2^{-2} are in good agreement with each other, but much narrower than that of the bulk (perfect crystal) component. The FWHM widths of the isotropic part of 2D-ACAR spectra are plotted against temperature in Fig.4 (b). The widths exhibit small increases at low temperature; upon cooling from 300K to 15K ,the broadening was about 1.5% for V_2^{-2} and V_2^{-1}, and 3.8% for V_2^0. It increases linearly with decreasing temperature for negatively charged divacancies, V_2^{-2} and V_2^{-1} which reflects lattice shrinkage and resulting increase in the positron-electron overlap around the divacancies. For the neutral divacancies, however, the ACAR-FWHM width shows an enhanced increase at lower temperatures below 200K.

The result of the positron lifetime measurements shows that the annihilation rate of positrons trapped

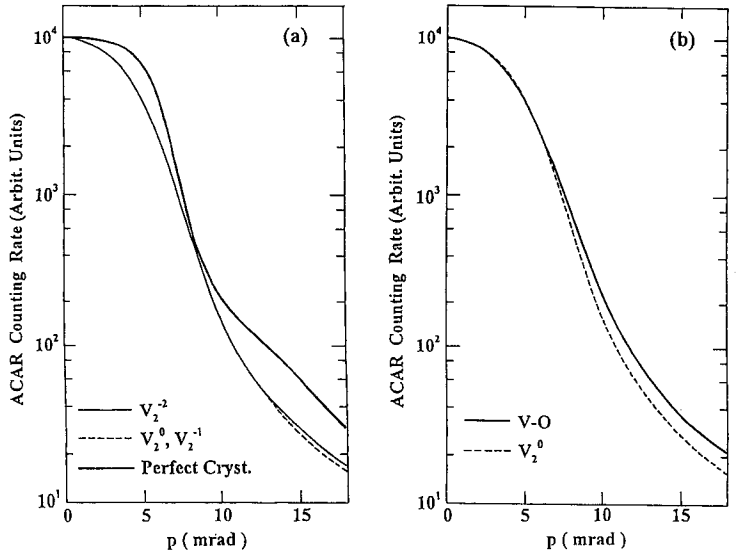

Fig.3. Isotropic parts of 2D-ACAR spectra with [0$\bar{1}$1] projection of (a) divacancies V_2^{-2}, V_2^{-1} and V_2^0, together with bulk component, and (b) V-O complex. These data are normalized to the same height at zero momentum.

at the negative divacancies increases linearly with decreasing temperature as shown in Fig. 4 (a). On the other hand the annihilation rate at the neutral divacancies is almost constant upon cooling. These different features of the positron annihilation characteristics, the ACAR-width and annihilation rate, between negative and neutral divacancies will be closely correlated to possible lattice relaxation around the divacancies. However clarification of them must await future theoretical studies.

We define a trapped fraction, ξ_t, as a ratio of the divacacy-trapped component intensity to the total ACAR component intensity. The trapped fraction at the divacancies increases with decreasing temperature, as shown in Fig. 5 for the neutral divacancies. The trapped fraction obtained from lifetime measurements using the simple trapping model is also shown. The fraction from the lifetime measurements shows very similar temperature dependence to that from the 2D-ACAR experiments [13,16]. However, the fractions from the lifetime are systematically larger than those from 2D-ACAR. A natural explanation for it will be that wave function of a positron trapped at the divacancy extends around the divacancy and has overlap with electrons in the bulk perfect crystal. The overlap gives partial annihilation with the electrons in the perfect crystal and hence an additional fraction in the lifetime experiments. In the analysis of the 2D-ACAR spectra we have assumed that all the characteristic anisotropies are arising from the bulk annihilation. Then we get higher trapped fraction from lifetime experiments as seen in Fig.5. However this explanation is not applicable to the negative divacancies; the trapped fractions from lifetime measurements were systematically smaller than those from the 2D-ACAR measurements on V_2^{-1} and V_2^{-2} as depicted in Fig.2 of our previous paper [12]. The discrepancy in the trapped fraction between the two experiments will give us useful information about positron localization at divacancies with various charge states as suggested in a theoretical study [23] and lattice relaxation around the divacancies.

It should be emphasized that the trapped fraction increases with decreasing temperature not only for the negative divacancies but also for the neutral divacancies [13,16]: at 295K ξ_t is 8.0% for V_2^0, 28.4% for V_2^{-1} and 17.2% for V_2^{-2}, and at 15K 59.7% for V_2^0, 68.6% for V_2^{-1} and 58.1% for V_2^{-2}. It can be explained by a phonon-cascade model [24] or weakly bound Rydberg state model [25] for negative divacancies, based on Coulombic attraction between the negative vacancy and a positron. However, the

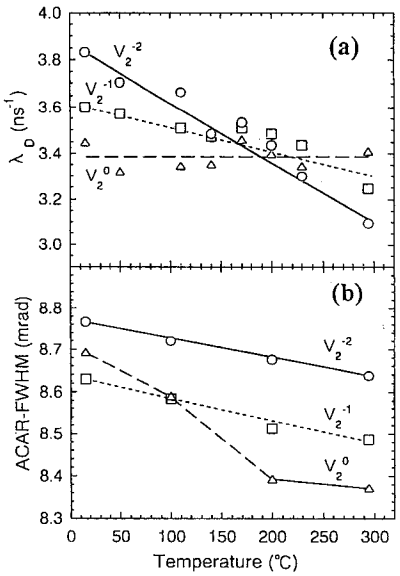

Fig.4. Temperature dependence of annihilation rate (a), and FWHM width of 2D-ACAR spectrum (b), of divacancies, V_2^{-2}, V_2^{-1} and V_2^0.

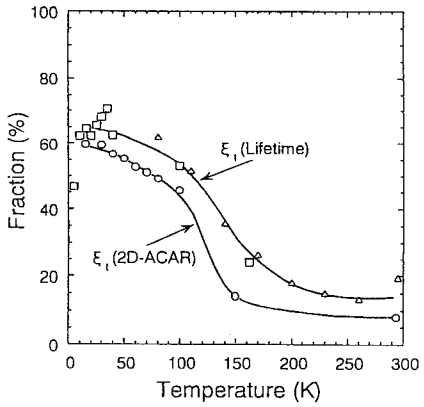

Fig.5 Temperature dependence of trapping fraction of neutral divacancies, estimated from 2D-ACAR and lifetime experiments. The different symbols, squares and triangles, denote results with different time spectrometers.

temperature dependence for the neutral divacancies cannot be interpreted by these models and remains unsolved [13].

2D-ACAR Spectra of Oriented Divacancies

As stated above, we have observed the nearly isotropic 2D-ACAR spectra from the divacancies. Our previous study shows actually that the anisotropy amplitudes relative to the trapped 2D-ACAR peaks are very small: 1.0% for V_2^0, 0.8% for V_2^{-1} and 0.8% for V_2^{-2} [12,13]. This smallness might seem somewhat unexpected, because the divacancies consist neighboring vacancies along <111> direction in the crystal and the resulting atomistic structure and hence the momentum distribution of the divacancies could be supposed to give large anisotropy. This small anisotropy of the trapped 2D-ACAR spectrum component is expected to provide us with useful information about electronic and microscopic structure in the divacancies. Then it is very necessary to obtain the detailed and definite structure of the anisotropy. The anisotropy, however, may be smeared by averaging with respect to four possible divacancy orientations: four equivalent <111> type orientations, [$\bar{1}$11], [111], [1$\bar{1}$1] and [11$\bar{1}$], as shown in Fig.6. Hence we prepared a specimen with oriented divacancies V_2^{-1} after Watkins and Corbett [19]. Watkins and Corbett have reported that alignment of the vacancy-vacancy axis direction of V_2^{-1} in the lattice can be achieved by stressing at elevated temperature, which was confirmed by electron paramagnetic resonance (EPR) experiments. By applying compression along [011] as stated above,

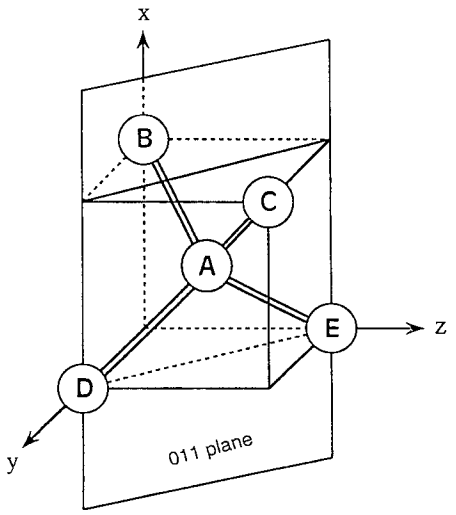

Fig.6. Crystal structure of Si and possible orientations of divacancies. To prepare the sample with oriented V_2^{-1}, compression stress was applied along [011] (B-C) direction. Divacancies along [1$\bar{1}$1](A-D) and [11$\bar{1}$](A-E) are "in-plane" , and those along [$\bar{1}$11](A-B) and [111] (A-C) are "out-of-plane " vacancies.

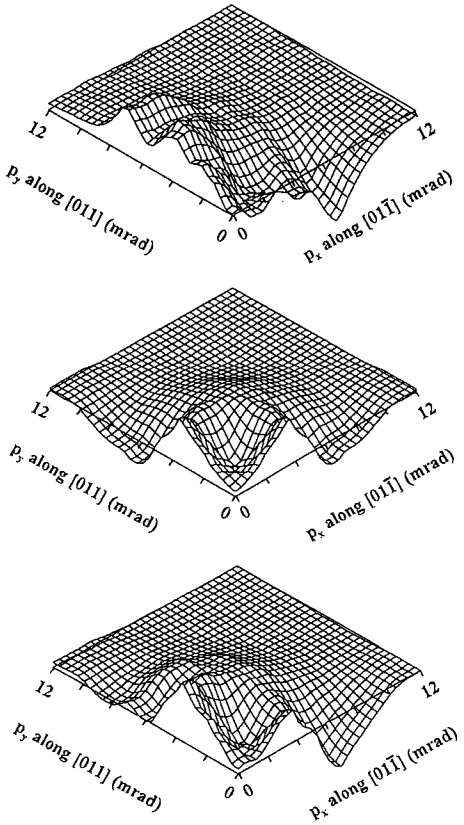

Fig.7. Anisotropies of 2D-ACAR spectrum of V_2^{-1} obtained by folding as described in the text: (a) after [011] and [01$\bar{1}$] folding, (b) after further folding along [010], (c) anisotropy of $A_{//}$.

some of the divacancies along [$\bar{1}$11] and [111] in the (01$\bar{1}$) plane change their orientation to [1$\bar{1}$1] or [11$\bar{1}$] direction in the (011) plane. The resulting polarization, n_{in}/n_{out} , is estimated to 1.5 from the experimental condition by Watkins and Corbett. Then the [01$\bar{1}$] and [011] directions are not equivalent. This inequivalence can be detected in the anisotropy of the 2D-ACAR spectrum. With the same procedure as described above, we got the divacancy components of the 2D-ACAR with [100] projection from 15K to 295K. These exhibit very small but definite tetragonal symmetries arising from the polarization. We summed all the divacancy components at various temperature to have better statistics. Then we obtained an anisotropy shown in Fig.7(a), after folding along [011] and [01$\bar{1}$] direction in the way of preserving the tetragonal symmetry.. We denote the anisotropy from the divacancies in the (011) plane, along [1$\bar{1}$1] and [11$\bar{1}$] direction, by $A_{//}$, while that from divacancies in the (01$\bar{1}$) plane, along [$\bar{1}$11] and [111] direction, by $A_{\perp}$. Figure 3(a) corresponds to $1.2\ A_{//} + 0.8\ A_{\perp} = 0.4A_{//} + 0.8(A_{//} + A_{\perp})$. Here we note that, to see the details of the anisotropy, it is multiplied by a factor of 2.34 as compared with that in Fig. 2. Figure 7(b) is the folding of Fig. 7(a) along [010] direction; we folded the anisotropy of Fig. 7(a) along [010] direction and got Fig.7 (b), which gives $(A_{//} + A_{\perp})$. Then we subtracted 2 times of Fig.7(b) from 2.5 times of Fig.7.(a) and obtained Fig. 7(c), which gives $A_{//}$. The amplitudes of the anisotropies relative to the 2D-ACAR peak heights are very small, 1.4% for (a), 0.9% for (b) and 1.8% for (c) of Fig. 7, while that of the anisotropy of the unirradiated specimen is 16.9% for the same orientation projection. It is noted that this anisotropy of the divacancy components is still a combination of those from the divacancies with two orientations, [1$\bar{1}$1] and [11$\bar{1}$], but because these divacancies are in reflection symmetry with respect to the (100) plane (perpendicular to the 2D-ACAR projection direction), they should show the same anisotropies. A small peak at about 3 mrad and a valley at about 7 mrad are seen along [01$\bar{1}$] direction, while a broad peak around 5 mrad along [011] direction. The question arises as to why so small anisotropy is observed even for the oriented divacancies. Here we mention two possible reasons. First Puska and Corbel [26] have shown, by a theoretical calculation with the method of superposing atoms, that in the case of divacancy the positron wave function is rather localized and isotropic as compared with that of single vacancy and have maximum amplitude in the middle of the two vacant sites. These feature of the wave function has been confirmed in a first-principles calculation by Saito and Oshiyama [27]. The isotropic positron wave function centered around in the middle of the two vacancies possibly cause isotropic momentum distribution. Second Saito et al. [28] have demonstrated that the lattice relaxation in the single vacancy bring about the isotropic momentum distribution. A very similar effect is also expected in the case of divacancies. We hope that the anisotropy, such as shown in Fig. 7(c) has an important information about the electronic structure of the divacancies, and encourages further studies including theoretical calculations.

V-O Complex

Behavior of vacancies in CZ-Si, having a large oxygen concentration, is more complicated than that in FZ-Si, having a low oxygen concentration, because of likely formation of the vacancy-complex with oxygen impurities in CZ-Si. We obtained the defect component of the 2D-ACAR spectrum of the electron-irradiated CZ-Si specimen after annealing at 300℃, in the same way as stated above . The resulting defect component was found to be very isotropic as the divacancy components. However, our previous study of positron lifetime measurements show that after annealing at 300℃ for 30 min major defects responsible for positron trapping are not divacancies but vacancy-oxygen complex, mostly divacancy-oxygen complex V_2O [18]; the defect component can be assumed to be due to the V-O complex. In Fig. 5(b) the V-O component is shown together with that of V_2^0. The V-O component shows almost the same distribution with that of V_2^0 at lower momentum region less than about 7 mrad, but enhanced at the higher momentum region, reflecting the broad momentum distribution of oxygen electrons and being expected to give useful information on electronic structure about the complex. It should be noted that the 2D-ACAR experiments has an advantage in the study of vacancy-oxygen complex because it gives precise and detailed momentum distribution in the higher momentum region. Detailed annealing studies of irradiated specimens are now in progress. It should be noted that recently a coincidence Doppler broadening method was successfully employed in the studies of higher momentum

region of vacancy-impurity complex in InP [29]. Then close comparison between two experiments, 2D-ACAR and coincidence Doppler, will be very interesting.

Summary

We have performed positron annihilation 2D-ACAR experiments on FZ-Si containing divacancies with definite charge states, -2, -1 and 0. Based on the characteristic anisotroppy in the 2D-ACAR spectrum of the bulk perfect crystal, the trapped component of 2D-ACAR spectra from the negative and neutral divacancies have been successfully separated from the observed 2D-ACAR spectra. The obtained 2D-ACAR spectra have been found to be almost isotropic and very similar to each other. Temperature dependence, from 15K to 295K, of the 2D-ACAR spectra from the divacancies has been also studied; the FWHM widths increase slightly with decreasing temperature, while the trapped fraction at the divacancies increases markedly at low temperature even for neutral divacancies. Using a sample containing oriented divacancies we have obtained small but definite anisotropies of the 2D-ACAR spectrum for the negative divacancies (V_2^{-1}). We have also got the 2D-ACAR spectrum from a vacancy-oxygen complex which shows enhanced distribution at higher momentum region. The 2D ACAR spectra distributions obtained in this study are expected to contains useful and potential information on the electronic structures and chemical surroundings of the divacancies in Si and await theoretical calculations to clarify the positron and electron states in the divacancies.

Acknowledgements.

We thank Dr. K. Masumoto and the technical staff of the Laboratory of Nuclear Science, Tohoku University , and Mr. H. Sunaga and Dr. S. Okada at JAERI Takasaki Institute for their help in electron irradiation. We also thank Prof. Y. Shirai and Mr. Y. Uno for their measurements of a part of the lifetime data shown in Fig. 5. We benefitted from discussion with Prof. P. Hautojärvi at Helsinki University of Technology. This work is partly supported by the Seki Memorial Foundation for Promoting Science and Technology.

References

[1] S. Dannefaer: "Defect Control in Semiconductors", Ed. by K. Sumino, (Elsevier Science, Amsterdam, 1990) p 1561.
[2] M.J. Puska: Mat. Sci. Forum **105-110** (1992) 419.
[3] P. Asoka-Kumar, K.G.Lynn and D.O. Welch: J.Appl.Phys. **76** (1994) 4935.
[4] P. Hautojärvi: Mat. Sci. Forum. **175-178** (1995) 47; J. de Phys. IV **5** (1995) C1-3.
[5] R.M. Nieminen: Mat. Sci. Forum **175-178**(1995) 279.
[6] Y.J. He, M. Hasegawa, R. Lee, S. Berko, D. Adler and A. Jung: Phys. Rev. **B33** (1986) 5924.
[7] S. Tanigawa: Mat. Sci. Forum **105-111** (1992) 493; Hyperfine Int. **79** (1993) 575.
[8] R. Ambigapathy, A.A. Manuel, P. Hautojärvi, Saarinen and C. Corbel: Phys. Rev. **B50** (1994) 2188.
[9] J.P. Peng, K.G. Lynn, M.T. Ulmor, D.J. Keeble and D.R. Harshman: Phys. Rev. **B50** (1994) 11247.
[10] A.A. Manuel, R. Ambigapathy, P. Hautojärvi, K. Saarinen and C. Corbel: J. de Phys.IV, **5** (1995) C1-73.
[11] A.A. Manuel, R. Ambigapathy, P. Hautojärvi, K. Saarinen and C. Corbel: Appl. Surf. Sci. **85** (1995) 301.
[12] T. Chiba, A. Kawasuso, M. Hasegawa, M. Suezawa, T. Akahane and K. Sumino: Mat. Sci. Forum **175-178** (1995) 327.
[13] M. Hasegawa, A. Kawasuso, T. Chiba, T. Akahane, M. Suezawa, S. Yamaguchi and K. Sumino: Appl. Phys. **A61** (1995) 65.
[14] A. Uedono, T. Kawano, X.H.Li, L. Wei, S. Tanigawa, A. Ikari, K. Kawakami, H. Haga and H. Itoh: Mat. Sci. Forum **175-178** (1995) 553.
[15] L. Gilgien, G. Galli.F. Gygi and R. Car: Phys. Rev. Lett. **72** (1994) 3214.
[16] A. Kawasuso, M. Hasegawa, M. Suezawa, S. Yamaguchi and K. Sumino: Hyperfine Int. **84** (1994) 397.
[17] A. Kawasuso, M. Hasegawa, M. Suezawa, S. Yamaguchi and K. Sumino: Mat. Sci. Forum **175-178** (1995) 423.
[18] A. Kawasuso, M. Hasegawa, M. Suezawa, S. Yamaguchi and K. Sumino: Jpn. J. Appl. Phys. **34** (1995) 2197.
[19] F. Bridges, G. Davies, J. Robertson and A.M. Stoneham: J. Phys. Condens. Matter **2** (1990) 2875.
[20] G.D. Watkins and J.W. Corbett: Phys. Rev. **138** (1965) A543.

[21] A. Kawasuso, M. Hasegawa, M. Suezawa, S. Yamaguchi and K. Sumino: Appl. Surf. Sci. **85** (1995) 280.
[22] T. Chiba and T. Akahane: "Positron Annihilation ", Ed. by L. Dorikens-Vanpraet, M. Dorikens, D. Seegers (World Scientific, Singapore, 1989) p674.
[23] M.J. Puska, O. Jepsen, O. Gunnarsson and R.M. Nieminen: Phys. Rev. **B34** (1986) 2695.
[24] S. Dannefaer, G.W. Dean, D.P. Kerr and B.G. Hogg: Phys. Rev. **B14** (1976) 2709.
[25] M.J. Puska, C. Corbel and R.M. Nieminen: Phys. Rev. **B41** (1990) 9980.
[26] M.J. Puska and C. Corbel: Phys. Rev. **B38** (1988) 9874.
[27] M. Saito and A. Oshiyama: Submitted to these proceedings.
[28] M. Saito, A. Oshiyama and S. Tanigawa: Phys. Rev. **B44** (1991) 10601.
[29] M. Alatarо, H. Kauppinen, K. Saarinen, M.J. Puska, J. Mäkinen, P. Hautojärvi and R. M. Nieminen: Phys. Rev. **B51** (1995) 4176.

Defects in Semiconductors 18
10.4028/www.scientific.net/MSF.196-201

Positron-Annihilation 2D-Acar Study of Divacancy and Vacancy-Oxygen Pairs in Si
10.4028/www.scientific.net/MSF.196-201.1481